



Enhancing 2D Deep Seismic Reflection Imaging Using Shot Domain Regularization: A Case Study from the Jiangnan Orogenic Belt, South China

Hui Zhang^{1, 2}, Jiayong Yan ^{1, 2*}, Zhendong Liu^{1, 2}, Jianguang Han^{1, 2}, Hao Wang³, Jiahao Liu¹

- 5 ¹Chinese Academy of Geological Sciences, Beijing, 100037, China.
 - ²State Key Laboratory of Deep Earth and Mineral Exploration, Chinese Academy of Geological Sciences, Beijing 100094, China.
 - ³China University of Mining and Technology (Beijing), Beijing, 100083, China.

Correspondence to: Jiayong Yan (yanjy@163.com)

Abstract: Deep seismic reflection is a key method for investigating plate tectonics, as it enables detailed imaging of lithospheric structures - particularly within the crust and upper mantle. It plays a crucial role in understanding crustal evolution and identifying mineral enrichment zones. However, during data acquisition, deviations from the planned shot and receiver locations often occur due to surface constraints or other logistical challenges. These deviations result in irregular seismic data that can introduce significant migration artifacts during processing, ultimately reducing data quality and hindering the interpretation of deep geological structures. To address this issue, we evaluated four data regularization strategies based on anti-aliasing Matching pursuit Fourier interpolation using a 2D deep seismic reflection dataset from the central Jiangnan Orogenic Belt. Among these, the method that involves regularizing and infilling shot gathers at 100-meter intervals produced the most effective results. Compared to legacy contractor-processed data, this method achieved a higher signal-to-noise ratio and improved seismic resolution. The superiority of that method was further confirmed through enhanced imaging in the prestack time migration results. These findings highlight the importance of shot domain regularization prior to migration in deep seismic reflection surveys.

1 Introduction

Deep seismic reflection has been recognized as an effective means to explore the continental basement and identify subtle lithospheric structures, which has been gradually applied to study the deep crustal structure and metallogenic processes (Krishna and Rao, 2005; Lü et al., 2013; Gao et al., 2014; Ahmadi et al., 2015; Naghizadeh et al., 2019; Liu et al., 2021). Because of this, a deep seismic reflection profile is often acquired in areas with rough topography, varying surface conditions, and complex tectonic geology. Consequently, Deep seismic reflection data are often sparsely and irregularly sampled across spatial coordinates due to both economic constraints and surface access limitations. This results in several processing challenges including uneven offset distribution, large offset intervals, and significant aliasing (Lan et al., 2021; Zappalá et al., 2024). In many cases, deep seismic reflection profiles exhibit poor stack quality in the shallow section, largely due to sparse





shot and receiver sampling and low signal-to-noise ratios (S/N). Therefore, migration of these data will inevitably generate unwanted migration artifacts, which adversely affect the interpretation of deep geological structures. Although deep seismic reflections primarily target deep structures, high-quality shallow seismic reflections are also crucial, as they provide valuable insights into the integrated relationship between shallow and deep structures.

35 Numerous researchers have conducted extensive studies on deep seismic reflection data pre-processing, time domain velocity analysis, and migration methods to enhance image quality (Snyder et al., 2008; Markovic et al., 2019; Ding and Malehmir, 2021; Liu et al., 2021; Lu et al., 2022). However, limited research has been conducted on the irregular sampling of deep seismic reflection data, and regularization of such data is rarely performed. The fold-based amplitude normalization method during migration was used to reduce unwanted migration noises and energy inequality (Zhu et al., 2014). Panea et al. (2017) used 2.5D acoustic finite-difference modelling to analyse the effect of a crooked line geometry on the S/N of deep seismic reflection data Panea et al. (2017), which indicated that irregular shot and receiver spacing introduced static time shifts into the arrival times of the reflected and head waves, lower S/N and some geologic interfaces of interest are not well-imaged. Interpolation of conventional seismic data on land allows under-sampled data to compensate for sparse acquisition, which could help to improve image quality (Bezerra et al., 2023). Nevertheless, interpolation of sparsely sampled deep seismic reflection data was often suboptimal using conventional frequency domain methods, as the aliased energy is likely to be chosen as signal (Wu and Xu, 2022). The anti-aliasing Fourier interpolation method was applied to regularize and infill shot gathers. The anti-aliasing capability of the method was achieved by first computing priors (spectral weights), which are typically derived from the lower frequencies of seismic data, and then used the computed weights to de-alias the higher frequencies (Schonewille et al., 2009). With the priors, real signals are much easier to select from the aliased data.

In 2019, a 2D deep seismic reflection crooked line was acquired by the China Geological Survey Project in the middle segment of the Jiangnan Orogenic Belt (JOB) (Liu et al., 2022). The intent of the project was to obtain a good subsurface structural image that can help understand the process of multi-stage collision, collage, breakup, and reconstruction of the South China continent (Jahn et al., 1990; Zhou and Li, 2000; Li et al., 2016; Gan et al., 2020; Hou et al., 2022; Hu et al., 2024; Lu et al., 2025). Meanwhile, it also helps determine the location of the underground metal abundance zones containing copper, tungsten, gold, and others (Xu et al., 2017; Yan et al., 2022). The survey line starts from Wuning, Hubei Province in the North and ends in Ji'an, Jiangxi Province in the South, with a total length of 200 km full-fold spread. Previously, both infield and in-house seismic data processing without seismic data regularization were performed by the contractors to obtain stack sections. And, the two results show low S/N overall, and the absence of clear reflections about major faults, the mountain area and its contact with the Basin that is the main target of the project.

In this paper, we proposed a target-oriented seismic pre-processing sequence and introduced anti-aliasing data regularization into the workflow. Four different data regularization strategies were tested and compared. The results demonstrate that the method of regularizing and infilling the shot gathers yields in a more regular and denser shot positioning as well as a more even offset distribution, which leads to higher fold, higher S/N, and better stack energy in both shallow and deep. Some dipping diffraction energy was better reconstructed with fewer artefacts. Benefits from the revised processing sequence, image quality



80



of the new pre-stack time migration provided less migration noises, and clearer images of shallow and deep underground geological structures in the middle segment of the JOB.

2 Geological and Geophysical Settings

The Yangtze Block and the Cathaysian Block merged in the early Neoproterozoic orogeny, forming the JOB (Li et al., 2019). The JOB can be divided into three major segments: the northeastern segment (Huaiyu or Shuangxiwu terrane), the middle segment (Jiuling terrane), and the southwestern segment (Xiangbei and Guibei terranes) (Wang et al., 2017). It is primarily composed of Meso-Neoproterozoic epimetamorphic strata, Neoproterozoic granite, minor mafic rocks, and contains two recognized Serpentinite belts (Fig. 1) (Yao et al., 2014; Yan et al., 2024). The formation of this geological unit is intimately associated with the amalgamation and subsequent breakup of the Rodinia supercontinent, representing a pivotal stratigraphic component within the South China Block (Mao et al., 2021; Chen et al., 2022). The JOB strata from the early to middle Neoproterozoic can be divided into two structural layers. The lower structural layer is the fold substrate, mainly composed of the Sibao Group, Fanjingshan Group, Lengjiaxi Group, Shuangqiaoshan Group, Shuangxiwu Group, and Xikou Group (Geng, 2015; Li et al., 2016). The upper structural layer is composed of the Heshangzhen Group, Dengshan Group, Likou Group, Banxi Group, Xiajiang Group, and Danzhou Group (Yao et al., 2019; Liu et al., 2025). The type of sedimentary construction is flysch formation, composed of greenschist facies metamorphic schist, argillaceous rocks, intercalated felsic tuff, spilite, and base-ultrabasic rocks(Zhang et al., 2021). The igneous rocks include a large number of peraluminous granites, as well as a small amount of mafic-ultramafic rocks and siliceous basalts (Wang and Li, 2003).

The present tectonic framework of the JOB since the Middle-Late Jurassic was formed under the combined effects of the Paleo-Pacific tectonic and intra-continental deep-seated structures, which is specifically manifested by the development of regional deep-seated faults and the presence of uplifted and depressed blocks segmented by these faults (Liu et al., 2022). The JOB has been shaped by multi-phase tectonism, resulting in a series of fault systems with distinct structural characteristics. The dominant faults in this region include the Pingxiang-Guangfeng Fault and the Yifeng-Jingdezhenn Fault. The Pingxiang-Guangfeng Fault is part of the Jiangshao Fault, which is the southern boundary of the JOB (Sun et al., 2018; Yao et al., 2019; Luo et al., 2022).

The survey line of the Wuning-Ji'an section is part of the middle segment of the JOB. It extends 200 km, starting from Jiugong Mountain Upheaval in the north, passing through the Xiushui-Wuning Basin, Jiuling Upheaval, Pingle Depression, and Wugongshan Upheaval in the south (Fig. 2) (Liu et al., 2022). The terrain along the survey line is characterized by a high northern section and a low southern section. The north of the survey line passes through Jiuling Mountain and Jiugong Mountain, which are mountainous regions with steep peaks, cliffs, and large lateral fluctuations, resulting in significant stratigraphic deformation. The relative elevation difference of Jiuling Mountain is 1000m, with slopes generally greater than 45 degrees. The south of Jiuling Mountain is a typical plain and hilly area with densely distributed towns, villages, and factories, and convenient transportation. These surface conditions posed challenges: the mountainous northern section made it difficult



105



to deploy a drilling rig and shots, while the densely developed southern section required modifications to the observation system.

The Sercel Lite 428 and the 20DX-10 Hz geophones were used for field seismic data acquisition, and a single group of 12 geophones was combined to receive seismic signals. The 20-24 kg shots were spaced at 200 m and performed in wells at depths of 20-30 m. The receivers were spaced at 40 m, totaling 800 channels with a full fold of 80. The trace spacing in a 12 km section of only the Xiuwu Basin was 20m, and the shot spacing and maximum offset were unchanged. Data were recorded with a 1 ms sampling interval over a 30 s record length. The survey line is crooked, it has two major bend points with angles of 19° and 4°. Although information such as satellite remote sensing, GIS information, and geological reconnaissance was comprehensively referred to in the design of the positions of the shots and receivers, the actual distribution of the shots and receivers still showed great irregularity and sparsity.

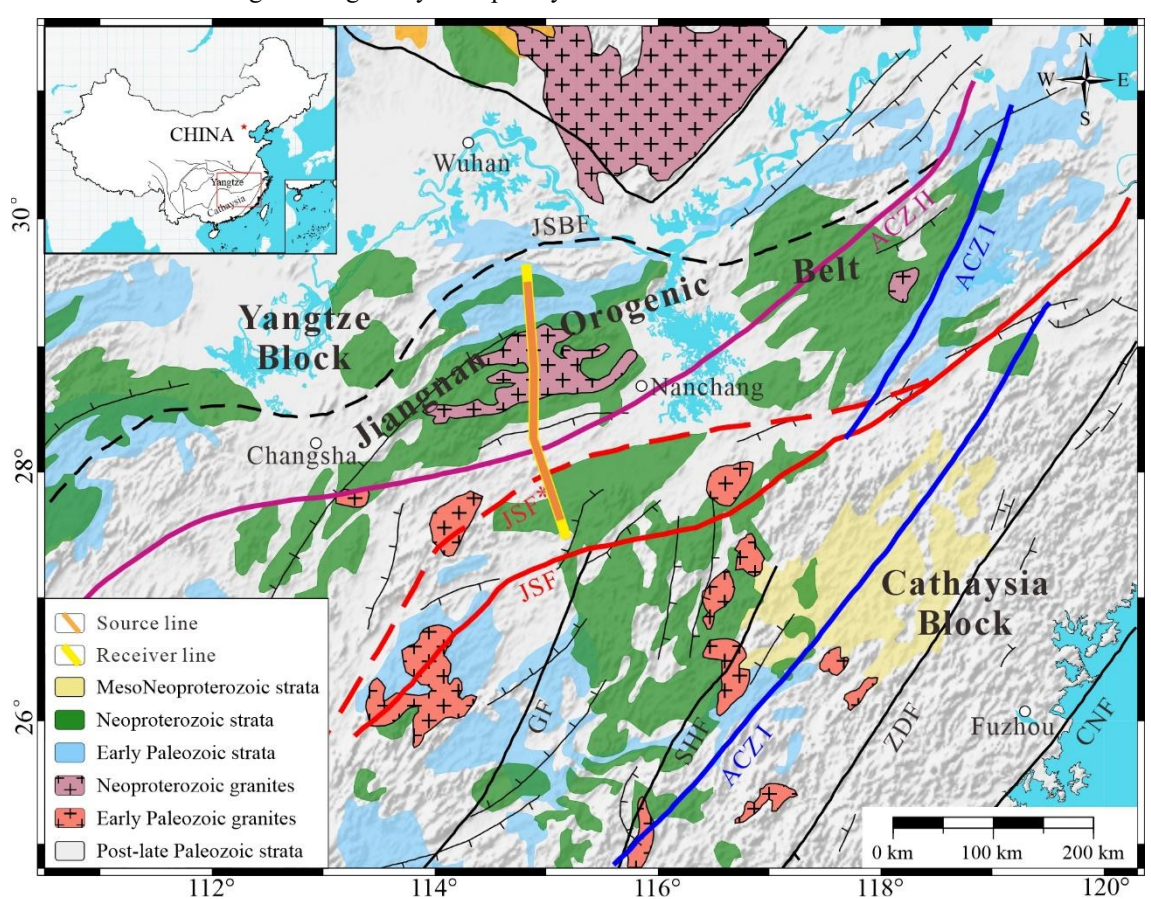


Figure 1 The location of survey line and geological sketch map of the study area (Yan et al., 2024). ACZ I: Ancient collisional zone of the Jinning period I, ACZ II: Ancient collisional zone of the Jinning period II, JSBF: Jiujiang-Shitai buried Fault, JSF/ JSF*:

110 Jiangshan-Shaoxing Fault, GF: Ganjiang Fault, SHF: Shaowu-Heyuan Fault, ZDF: Zhenghe-Dapu Fault, CNF: Changle-Nanao Fault





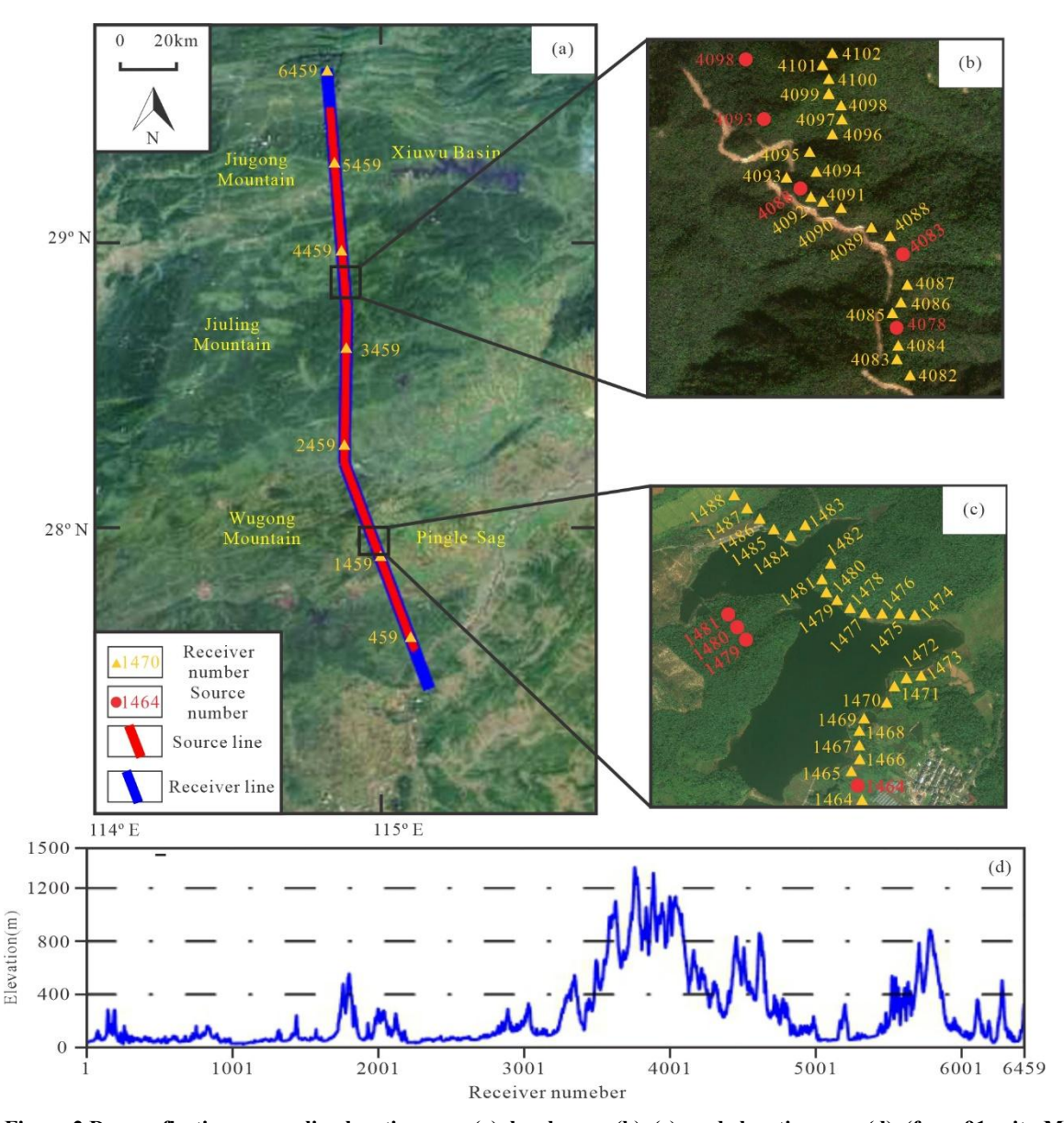


Figure 2 Deep reflection survey line location map (a), local maps (b), (c), and elevation map (d). (from 91weitu Maps)

115 3 Target-oriented Seismic Data Pre-processing

120

The primary goal of deep seismic reflection exploration is to reveal complex underground tectonic structures. Generally, near-surface conditions in these target areas are highly complex. The targets of exploration are located 30-100 km beneath the surface or even deeper, making seismic wave propagation paths considerably long and wave fields extremely complex. Field acquisition for deep seismic reflection is primarily conducted along 2D survey lines. This typically involves long arrays with large offsets, ranging from 16-20 km, and offsets for larger shots can extend up to 50 km. Receivers spacing is relatively large,





generally 40-50 m, while shot spacing is typically 200-300 m. The distribution of the shots and the receivers is irregular. The acquired data often exhibit inconsistent amplitude energy and weak effective reflection energy. Moreover, significantly high-frequency attenuation of deeper signals coupled with the pervasive presence of background noise results in a low S/N. Therefore, it is necessary to adopt targeted processing technology for deep seismic reflection data. In this study, targeted processing was applied to a 2D deep seismic reflection data located in the middle segment of the JOB (Wuning-Ji'an section). Table 1 outlines the main processing steps employed in this work.

Table 1. Deep reflection seismic processing flows

Processing Steps	Methods
Reading SEGD files	
Geometry definition	Common center point centroid smoothing method.
Static corrections	Refraction and tomography static correction (ultimately adopting the tomography method)
Noise attenuation	Abnormal amplitude attenuation in multi-domain and multi-frequency bands, non-uniform coherent noise suppression (NUCNS), and curved wave transform noise attenuation.
Deconvolution	Robust surface consistent pulse deconvolution based on spectral constraint
Velocity analysis	Velocity analysis combines velocity spectra and constant/variable velocity scanning.
Residual Statics	Surface consistent reflection residual statics and residual statics of a large window Monte Carlo simulation based on simulated annealing algorithm.
Data Regularization	Matching pursuit Fourier interpolation (MPFI)
Migration	Kirchhoff Pre-stack time migration
Stack and Display	





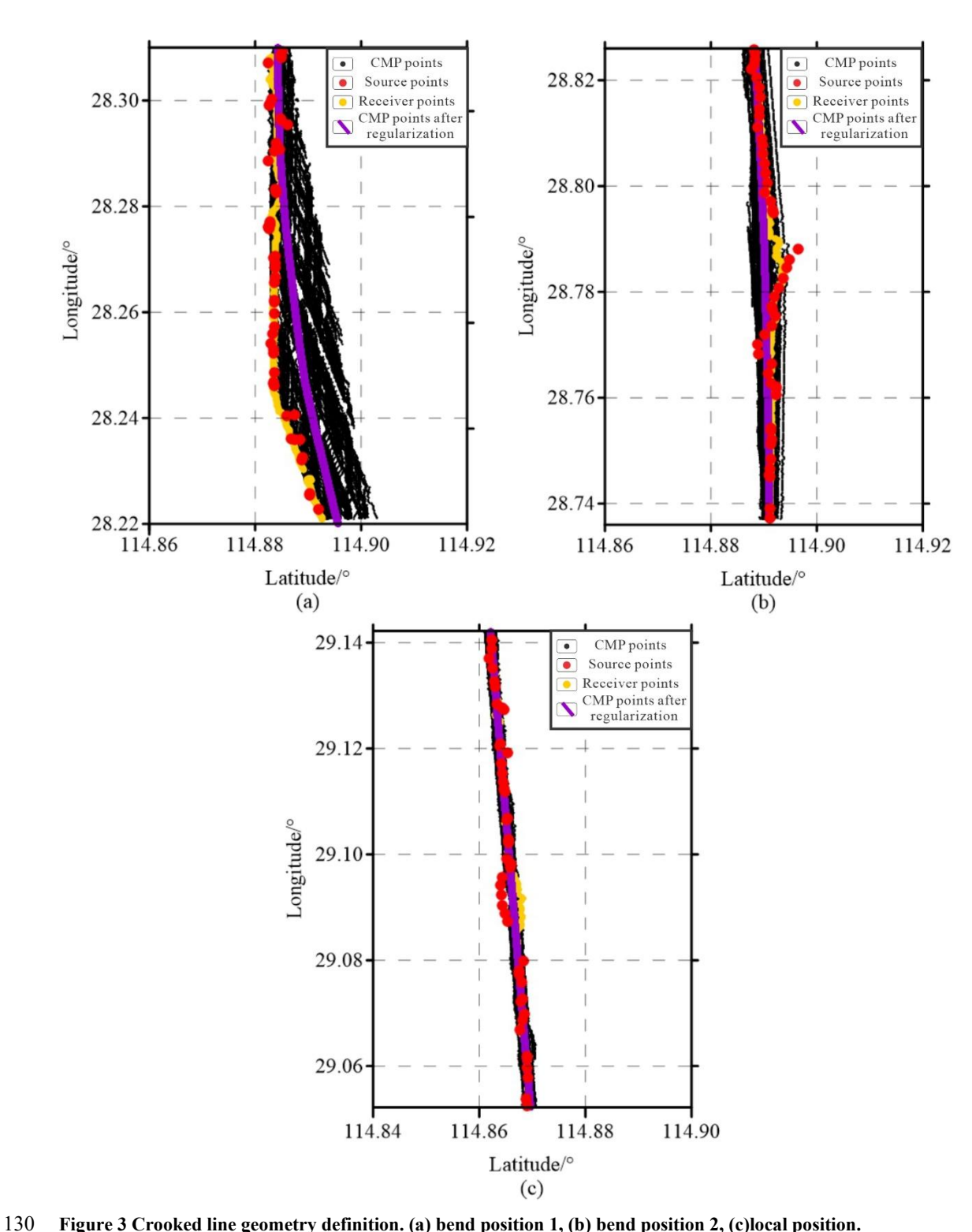


Figure 3 Crooked line geometry definition. (a) bend position 1, (b) bend position 2, (c)local position.



140

145

150

155

160



3.1 Geometry Definition

In a regular 2D linear seismic observation system, the spacing between shots and receivers is uniform. They are deployed along a straight line. Consequently, the locations of common midpoints (CMP) converge into cell centers of linear observation system. However, the deep seismic reflection survey line in this study was deployed using crooked lines with two main bend positions, and the shot and receiver distribution was irregular. These resulted in the dispersion of CMP, forming a planar distribution. Therefore, the CMP gathers represent reflection surfaces in the subsurface rather than reflection points. As shown in Figure 3, yellow marks the receivers, red marks the shots, and black indicates the dispersed CMP. While defining a crooked line observation system does not directly reduce the dispersion of CMP, suitable cell center positions can effectively attenuate CMP dispersion effects. The cell center positions for the crooked-line observation system were determined using the Common center point centroid smoothing method to completely solve this problem. Initially, cell center positions were established based on a fixed CMP spacing, typically half the receiver spacing. Next, the centroid of the CMP near each initial cell center position was calculated, and the centroid positions were smoothed according to a specified scale, resulting in a crooked line. Finally, the appropriate starting position for the cell center was selected, typically the midpoint between the shot and the receiver. The final cell center positions were then determined along the crooked line using equal CMP spacing (as shown in purple in Fig. 3). This method ensured that the CMP strike was aligned along the survey line, better representing the distribution of CMP and the actual position of subsurface reflections.

3.2 Static Correction

P-wave velocity tomography inversion is employed to derive the near-surface velocity structure using the first-arrival wave travel times from deep seismic reflection. The method has been extensively applied in both oil exploration and deep seismic reflection data processing, owing to its ability to provide high-resolution models of complex near-surface conditions (Zhu et al., 2014; Gonçalves and Garabito, 2021). Both refraction static correction and tomography static correction methods were tested to evaluate the effectiveness of tomography static correction (as shown in Fig. 4). The results indicate that tomography static correction (Fig. 4c). outperform refraction static correction (Fig. 4b), particularly in regions characterized by significant surface elevation variability. Based on these findings, tomography static correction was selected for further application in this study.

The first-arrival times were meticulously picked from the full array to ensure the accuracy of subsequent analysis. A subsurface velocity model was inverted by establishing the linear equation relating the slow-wave perturbation, based on a ray-tracing technique that accounts for complex spatial velocity variations. The final datum surface was established at 1500 m, with a replacement velocity set at 5000 m/s. The method addressed medium short and long wavelength static anomalies caused by near-surface irregularities. It effectively corrected distortions in first-arrival times and in-phase axes, which were critical for enhancing the continuity and accuracy of seismic reflection data.





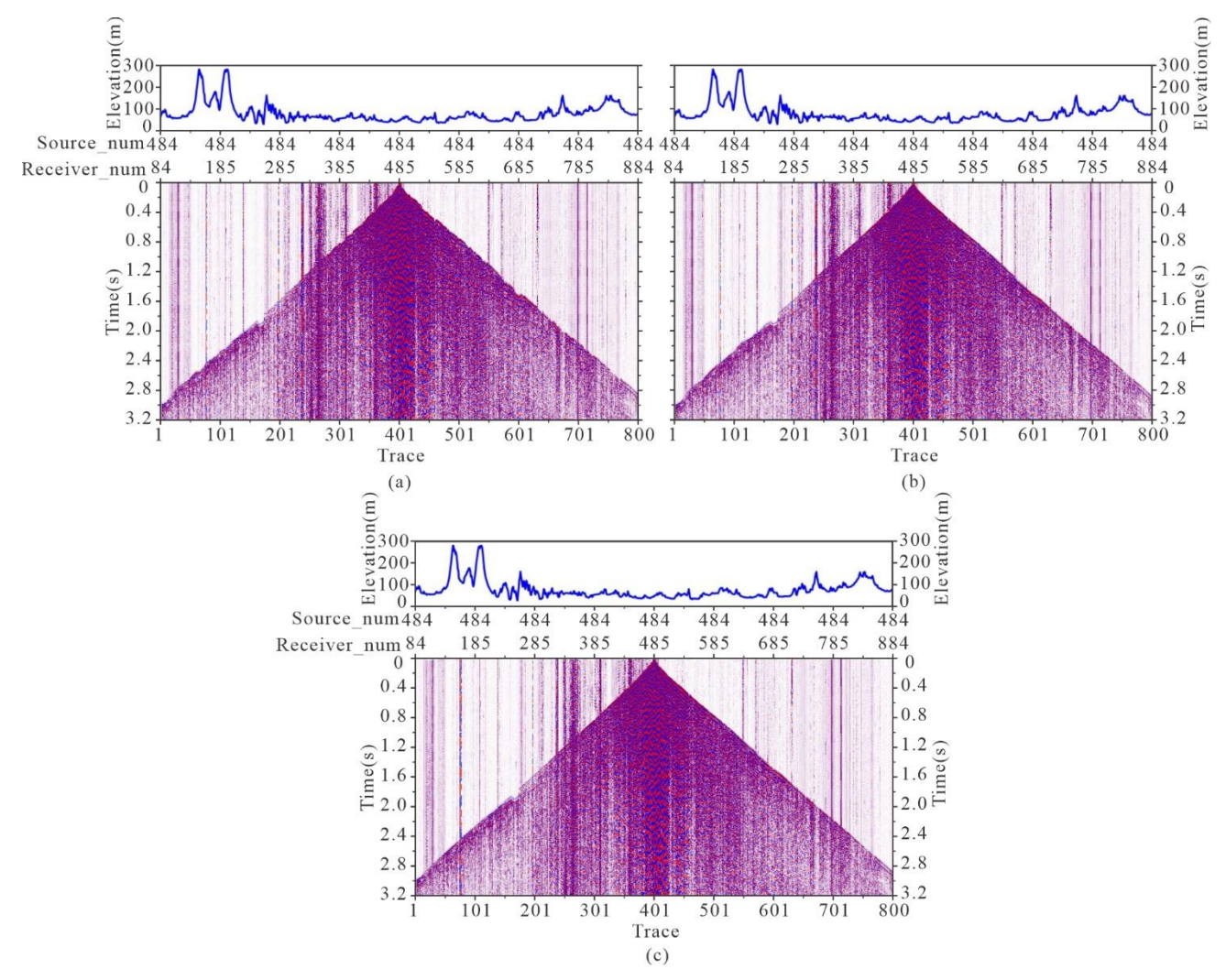


Figure 4 The shot gathers before and after static correction. (a) the original shot gather, (b) the shot gather after refraction static, (c) the shot gather after tomography static

3.3 Noise Attenuation

170

Deep seismic reflection data were affected by a variety of noise, including surface waves, linear interference, and background noise (Fig. 5a). A comprehensive multi-step noise attenuation approach was employed to mitigate these noise components and enhance the quality of the data. First, amplitude attenuation was applied to abnormal signals in three domains: the shot domain, the receiver domain, and the CMP domain. This step focused on safeguarding the effective seismic signal while eliminating abnormal noise at boundaries. Specifically, the median energy was calculated by counting the amplitudes across multiple frequency bands within a specified time window. Amplitudes exceeding a predefined threshold in any frequency band were identified as abnormal noise and appropriately attenuated. Next,



180

185

190

195



NUCNS that combines with the least-squares optimization method and F-X sector filter in the frequency domain, was used to suppress local coherent noise. For each receiver, a linear interference model was independently estimated within a specified velocity range, allowing for precise noise reduction tailored to local conditions. Finally, advanced analysis in the curvelet wave domain was conducted to differentiate between effective reflection waves and interference waves. This process involved decomposing seismic signals into 6 frequency bands, 50 angles, and the spatial domain to isolate and preserve effective wave information. As a result of these denoising processes, surface waves and other noise were significantly attenuated, improving S/N. This enhancement not only facilitated clearer imaging but also ensured the data are well-prepared for subsequent processing (Fig. 5).

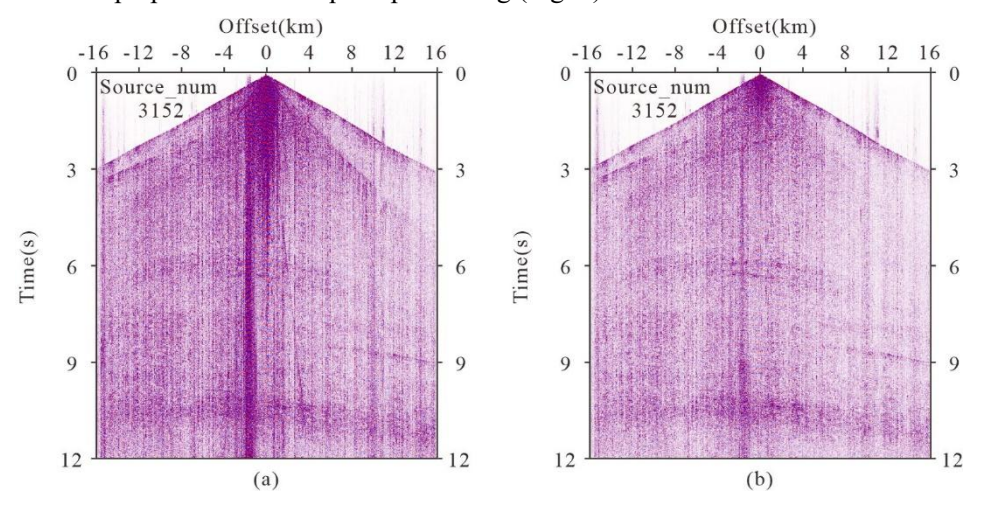


Figure 5 The shot gathers before (a) and after (b) noise attenuation.

3.4 Deconvolution and Residual Statics

The lateral heterogeneity of near-surface conditions, coupled with the variability introduced by excitation and reception factors, leads to significant differences in seismic data energy and wavelet consistency. Deep seismic reflection data often emphasize low-frequency information, which is critical for capturing the true response of deep strata (Taner and Koehler, 1981; Cary and Lorentz, 1993; Kazemi et al., 2016). The conservative noise suppression approaches were employed, aiming to suppress noise while retaining effective reflections. Despite this, the inherently low S/N of the data and the potential for residual local noise necessitated additional measures to enhance data quality. The robust surface consistent deconvolution was adopted to address these challenges. The method integrates amplitude and phase constraint signal processing workflows, which can simultaneously obtain the amplitude compensation factor and deconvolution operator of surface consistency to provide relative amplitude preserved data. At the same time, additional noise attenuation feature allows automatic identification of high amplitude surface inconsistent noisy zones. It attacks the inconsistent noise using Jacobi with over-relaxation, able to give unbiased results even in the presence of strong outliers due to inconsistent noise. Therefore, the spectrum constrained robust surface consistent pulse deconvolution was performed. The main parameters included: 1 ms predictive step and 240 ms





operator length. As demonstrated in Fig. 6, the post-deconvolution data exhibit improved energy uniformity across shot points, along with enhanced strength of the effective wave signals.

Surface consistent reflection residual statics and residual statics of large window Monte Carlo simulation based on simulated annealing algorithm were utilized to solve the residual short-wave length statics after noise attenuation and surface consistent deconvolution. The residual static correction and velocity analysis were iterated 5 times. The final iteration residual statistics converged more than 95% in one sample, and the continuity of the reflection wave in the phase axis was improved. Furthermore, the stacking process benefited substantially from the modified statics.

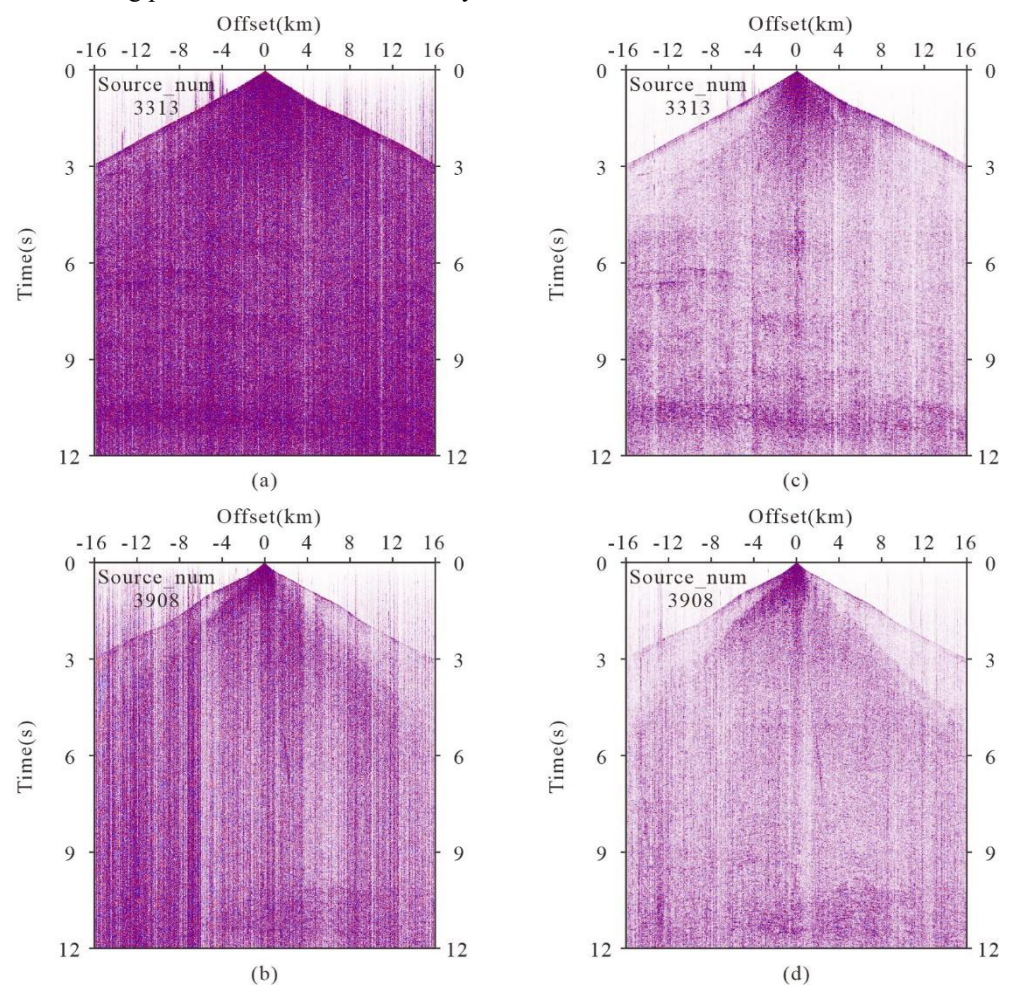


Figure 6 The shot gathers before (a), (b), and after (c), (d) robust surface consistent deconvolution.

4 Deep Seismic Reflection Data Regularization

The Matching Pursuit Fourier Interpolation (MPFI) is a frequency-domain method that employs Fourier transforms as the dictionary or basis functions. The seismic data need to be transformed from the space-time domain to the space-frequency





domain by the Fast Fourier transform (FFT). This approach enables the decomposition and analysis of seismic signals in the frequency domain, effectively extracting characteristic information from the reflection signal. The conventional MPFI algorithm iterates over irregular seismic data multiple times, redistributing leaked energy from other Fourier coefficients back to the original ones. If aliasing energy exceeds effective wave energy, it may be incorrectly chosen as the best atom, thereby affecting the interpolation result. To address this issue, the energy at various dips in the low-frequency band of seismic signals is calculated and used these values as weights (prior value) for the Fourier spectrum of the high-frequency band. Higher weights are assigned to genuine seismic signals, while lower weights are given to alias frequency signals (Fig. 7). Consequently, alias frequency energy exceeding real signal energy is not erroneously selected as the maximum in each iteration, effectively eliminating spatial alias frequencies (Schonewille et al., 2013). The specific steps of the algorithm are as follows:

- a) The FFT and the Discrete Fourier transform (DFT) are used to convert irregular deep seismic reflection data from the space-time domain to the frequency-wavenumber domain;
- b) The energy curves at various dips in the low-frequency band for the Fourier spectrum are computed and utilized as weighting factors applied to the entire Fourier spectrum;
- c) Identify the Fourier spectrum component with the highest energy after weighting (effective signal);
- d) Integrate this component into the original Fourier spectrum without weighting;
- e) Perform an inverse Fourier transform on the Fourier spectrum component obtained in the preceding step and output the result to the corresponding original input positions;
- f) Subtract the iterative result from the (5) step from the original input data to proceed with the next iteration; According to the set number of iterations or threshold, repeat steps (2)-(6), and get the expected results.

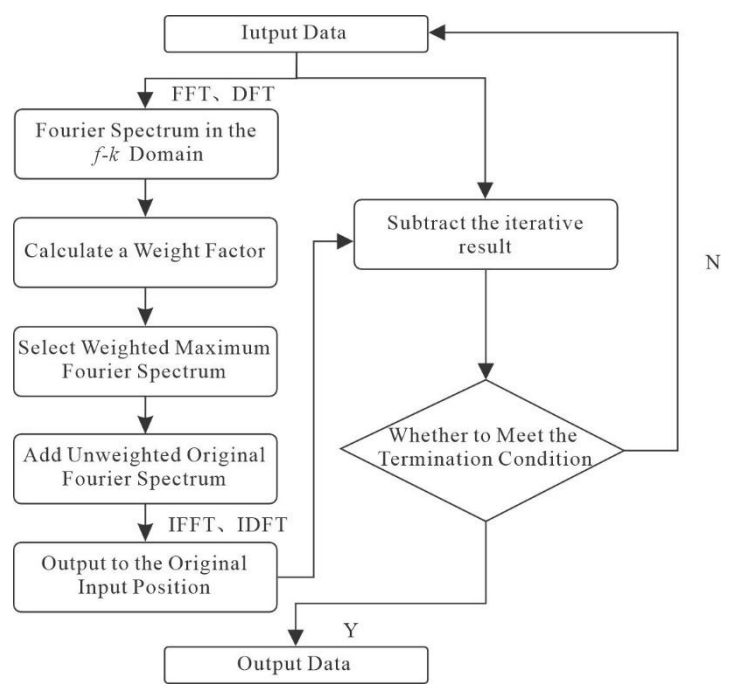


Figure 7 MPFI workflow diagram.

220

210

215

225



235

240

245

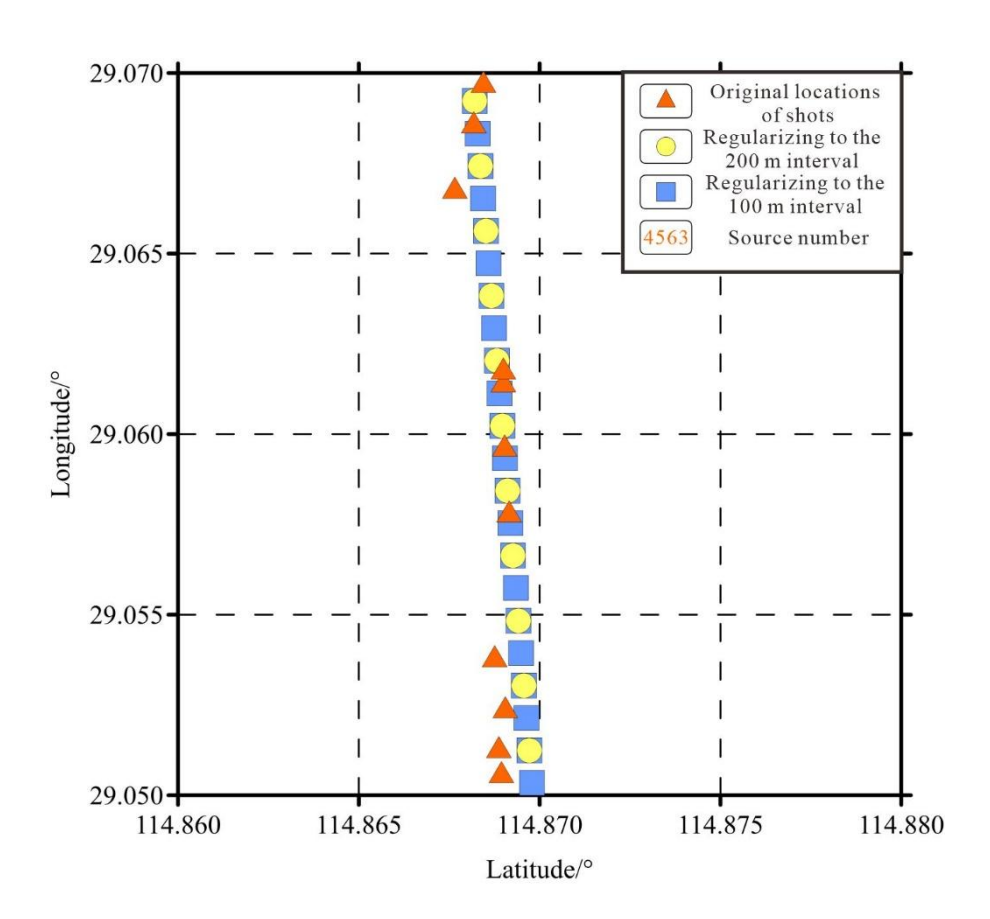
250



- The above method is not only suitable for two-dimensional seismic data, but also can get a better processing effect for high-dimensional seismic data. To evaluate the degree of improvement that regularization can bring to deep seismic reflection imaging, four regularization methods were designed using the MPFI algorithm. The details are as follows:
 - 1) Infilling "gaps" in the offset domain while shot locations remain irregular: In the method, seismic data were sorted according to the common offset to generate a data volume within the offset domain. Due to the irregular distribution of shots and receivers, certain portions of the data volume contained "gaps", where seismic traces were missing. These "gaps", caused by irregular sampling, were infilled by interpolating the missing seismic trace positions. The results (Figs. 10b and 11b) showed moderate improvement in the seismic profiles, with fold increasing to around 100.
 - 2) Full regularization in the offset domain: The method involved fully regularizing all data within the offset domain, where the CMP locations were restored to their pre-designated positions (the cell center locations). This ensured a uniform distribution of seismic traces across each offset. The results (Figs. 10c and 11c) showed an improvement over the "infilling gaps" method (Figs. 10b and 11b), with better alignment and consistency in the seismic profiles. The fold was generally around 80, with local areas slightly exceeding 80.
 - 3) Regularizing shot positions to a 200 m interval in the shot domain: In the method, the seismic data were sorted according to the same shot gathers to create a data volume within the shot domain. The irregularly distributed shots were adjusted and restored to their pre-designed positions by the method (Fig. 8). The results (Figs. 10d and 11d) demonstrated that regularization in the shot domain yields improvements over previous methods. The processed profiles exhibited a higher S/N and clearer imaging. Additionally, the uniformity of fold was maintained at 80.
 - 4) Regularizing shot positions and infilling shot gathers to a 100 m interval in the shot domain: The method infilled shot gathers to a 100 m interval based on Method 3). As shown in Fig. 9, the infilled shot gather (Fig. 9d) was similar to the adjacent original shot gather (Fig. 9c, and 9e). It was evident that the shot gathers after regularizing and infilling (Fig. 9c, 9d, and 9e) exhibit better quality than the original shot gathers (Fig. 9a and 9b), with more prominent effective waves. Moreover, the stacked profiles of both shallow and deep areas (Figs. 10e and 11e) were better than those without infilling shot gathers. The uniformity of fold was maintained at 160.







255 Figure 8 The shot locations before and after regularization





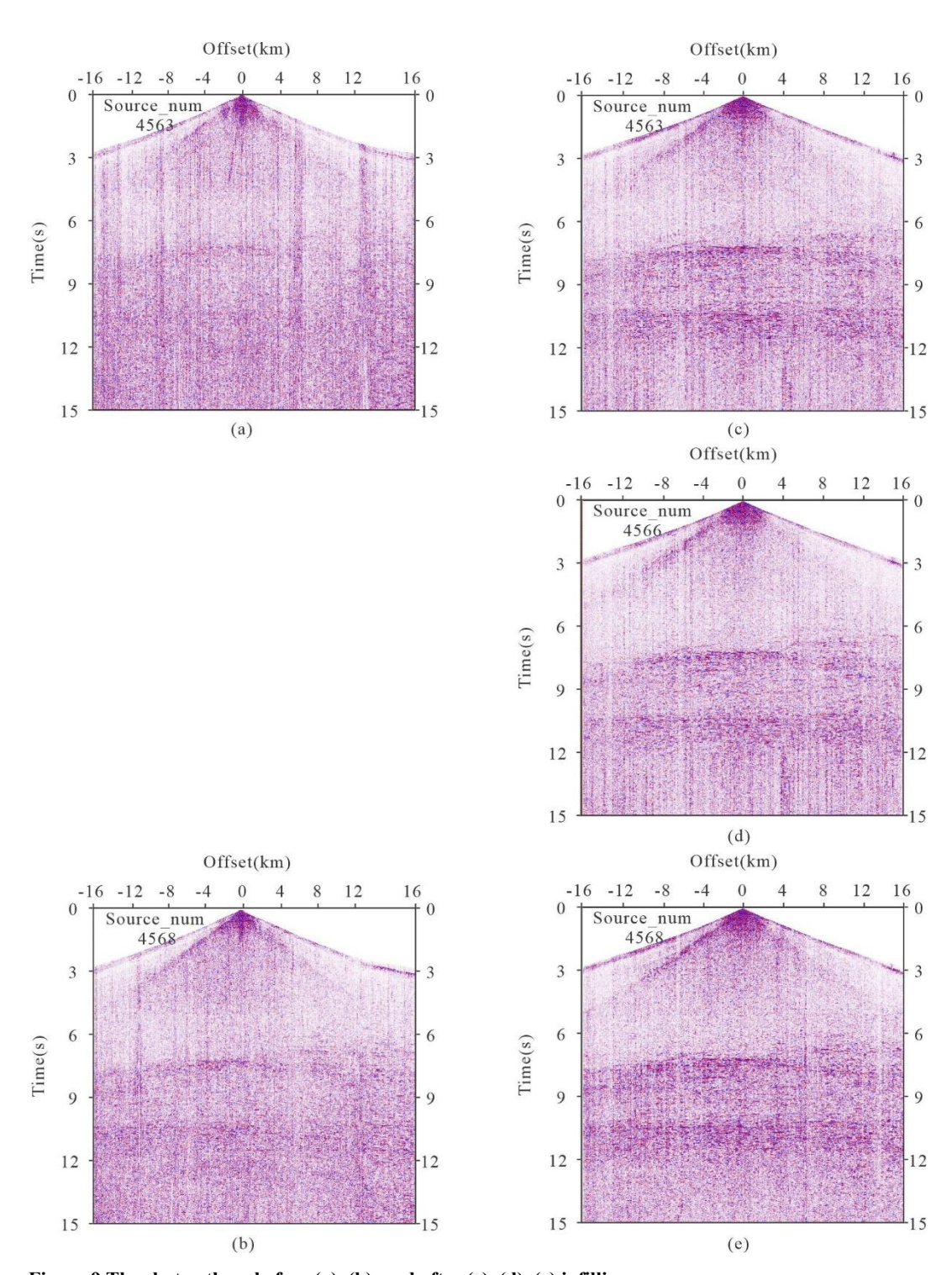


Figure 9 The shot gathers before (a), (b), and after (c), (d), (e) infilling.





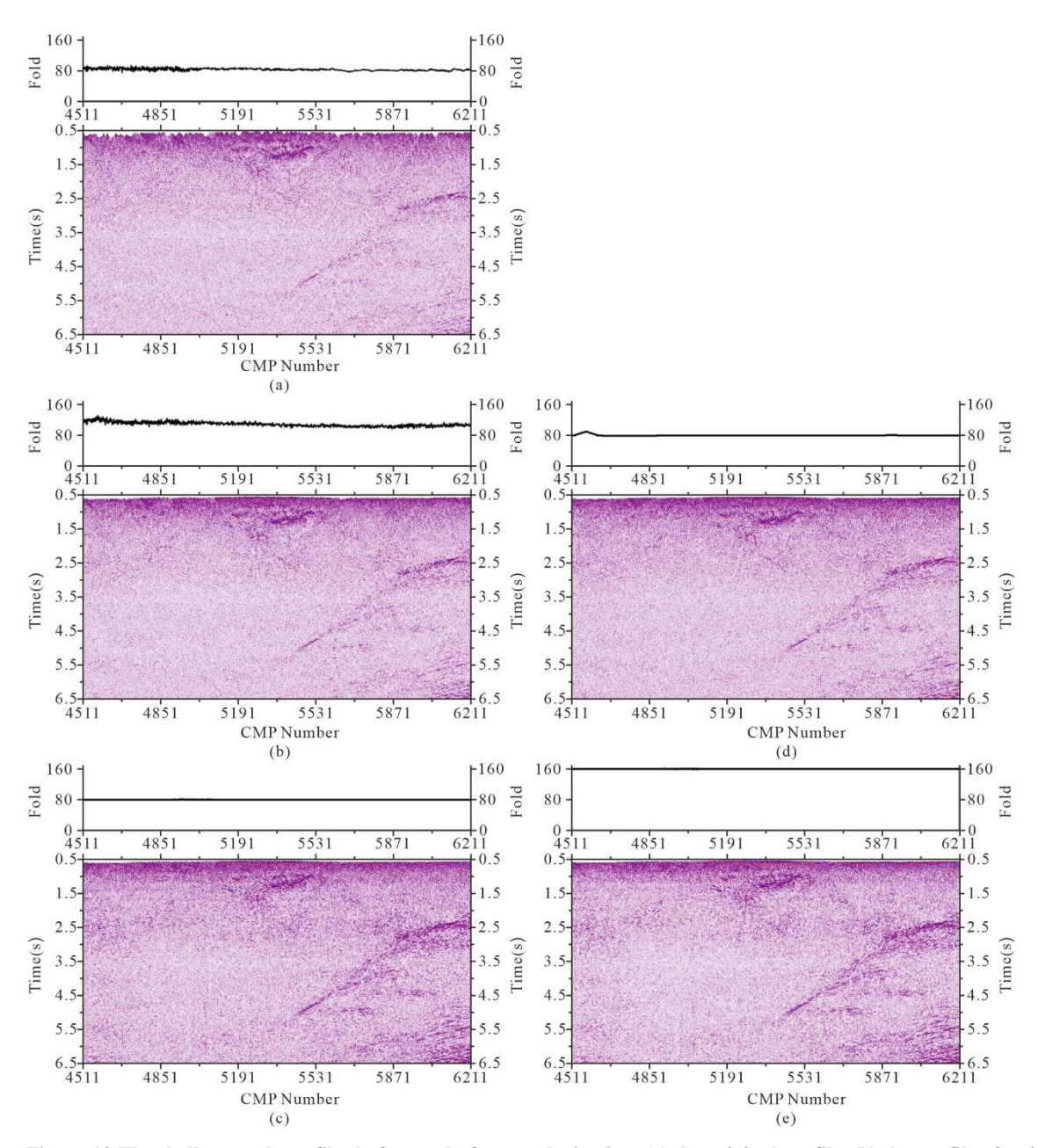


Figure 10 The shallow stack profiles before and after regularization. (a) the original profile, (b) the profile after infilling gaps in the offset domain, (c) the profile after full regularization in the offset domain, (d) the profile after regularization in the shot domain, (e) the profile after regularization and infilling shot gathers in the shot domain.





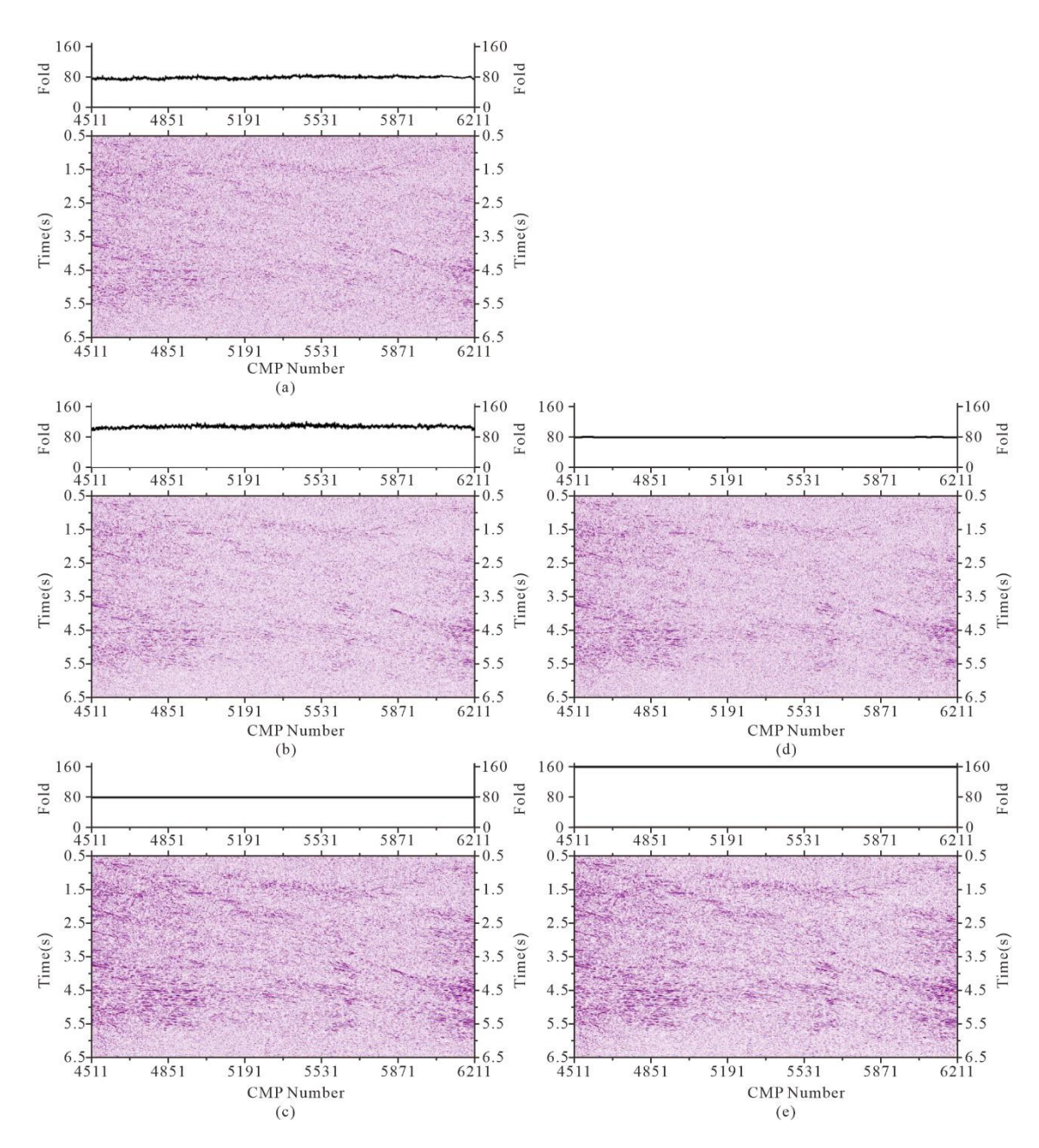


Figure 11 The deep stack profiles before and after regularization. (a) the original profile, (b) the profile after infilling gaps in the offset domain, (c) the profile after full regularization in the offset domain, (d) the profile after regularization in the shot domain, (e) the profile after regularization and infilling shot gathers in the shot domain.

5 Discussion

270

The results presented in Figs. 10 and 11 demonstrate that regularization enhanced the image quality of seismic profiles in both shallow and deep regions. Among the methods tested, the regularization in the shot domain consistently outperformed that in



275

280

285



the offset domain, obtaining higher S/N and clearer profiles. Although regularization in the offset domain can reposition the CMP locations onto the pre-designed curved line, the actual spatial coordinates of the corresponding shot and receiver positions still shift during the CMP spatial adjustment. In contrast, regularization in the shot domain physically relocates the shot points directly to their designed acquisition coordinates, making it more "physically" meaningful in implementation. Therefore, the processing in the shot domain obtained superior results, particularly when regularizing and infilling shot gathers to a 100 m interval.

Fig. 12 and 13 show that the Method 4) proposed in this paper improved the stack profiles quality and enabled clearer identification of major structure within the study area, compared with processing by the two contractors. The profile from Contractor A has a low S/N, and the reflections of the main faults and rock masses are not prominent. Although the profile obtained from Contractor B displays the target reflection wave group, the resolution of specific features is notably inferior to that achieved through regularization-based processing. This improvement was most evident in the profiles of pre-stack time migration (Fig. 14 and 15), where the structural clarity and continuity were enhanced following regularization with infilling shot gathers to a 100 m interval. It is worth noting that the effects of regularization were slightly less in the deep regions compared to the shallow areas. This may be attributed to the attenuation of seismic signals with increasing depth, which weakens the effective signal and limits the improvements achievable through regularization. In summary, regularization in the shot domain, with infilling shot gathers to a 100 m interval, proved to be the most effective approach for improving seismic imaging quality. These findings highlight the importance of tailored regularization strategies in addressing specific challenges associated with deep seismic reflection data.





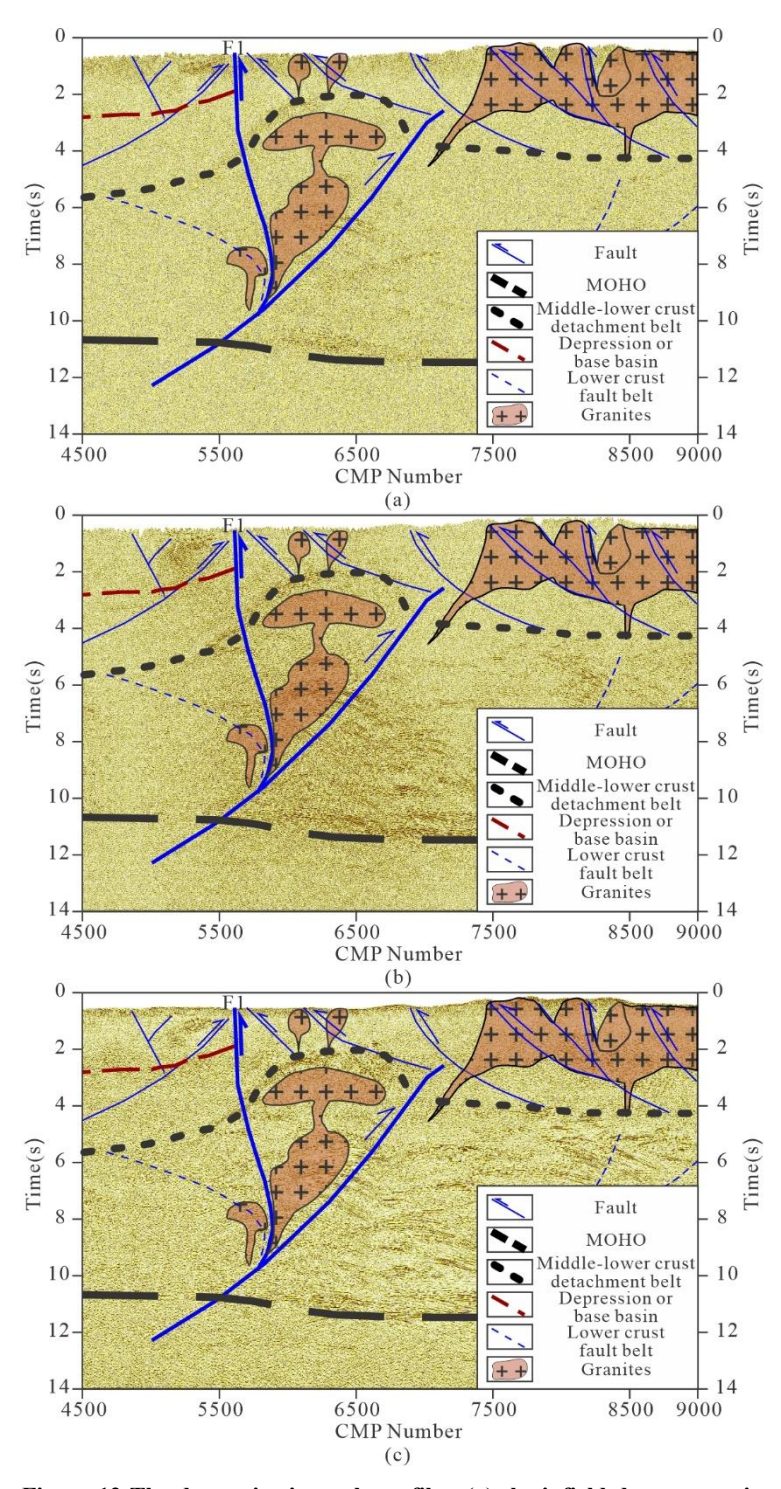


Figure 12 The deep seismic stack profiles. (a) the infield data processing from the contractor A, (b) the in-house data processing from the contractor B, (c) the data processing after regularization and infilling shot gathers in the shot domain, F1: Yifeng-Jingdezhen Fault.

19





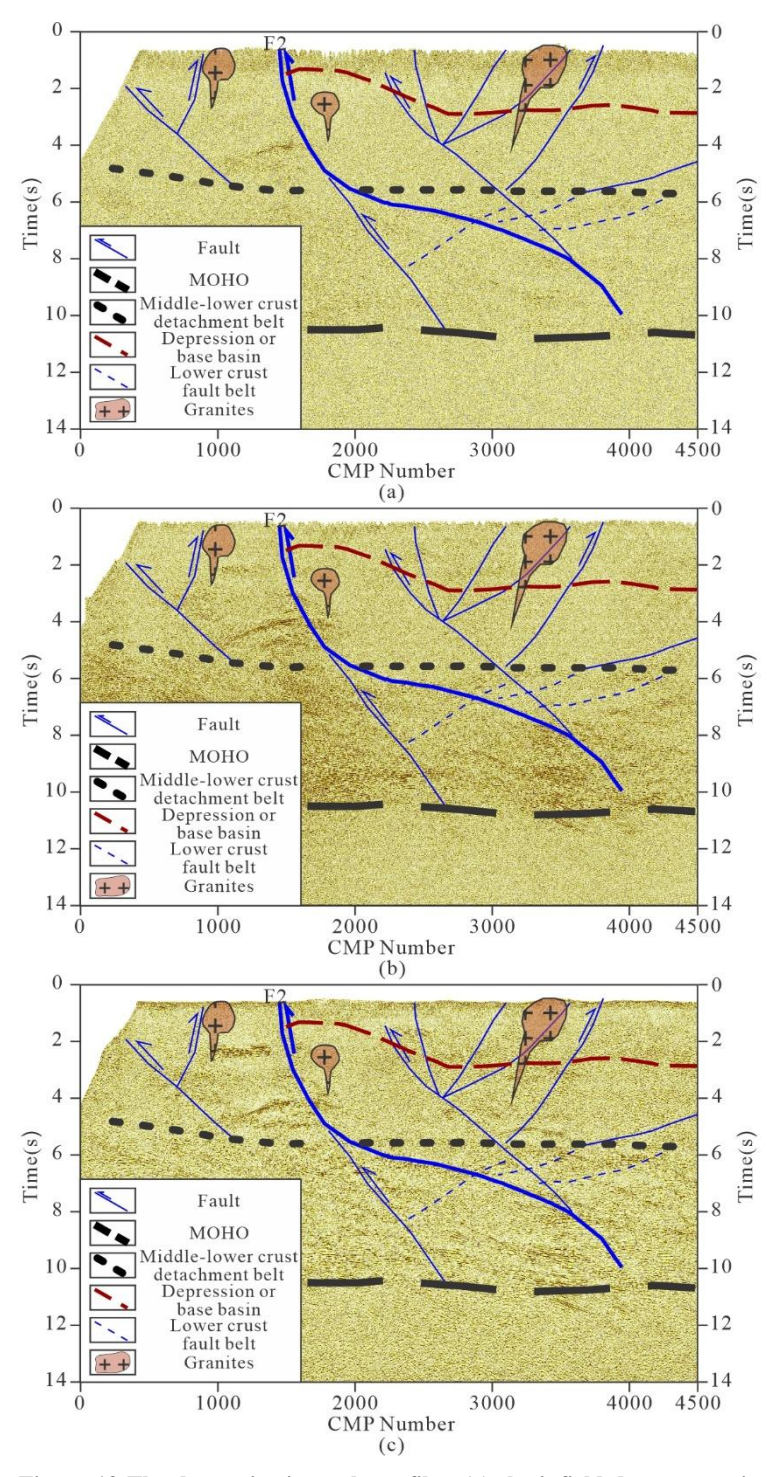


Figure 13 The deep seismic stack profiles. (a) the infield data processing from the contractor A, (b) the in-house data processing from the contractor B, (c) the stack profile after regularization and infilling shot gathers in the shot domain, F2: Pingxiang-Guangfeng Fault..





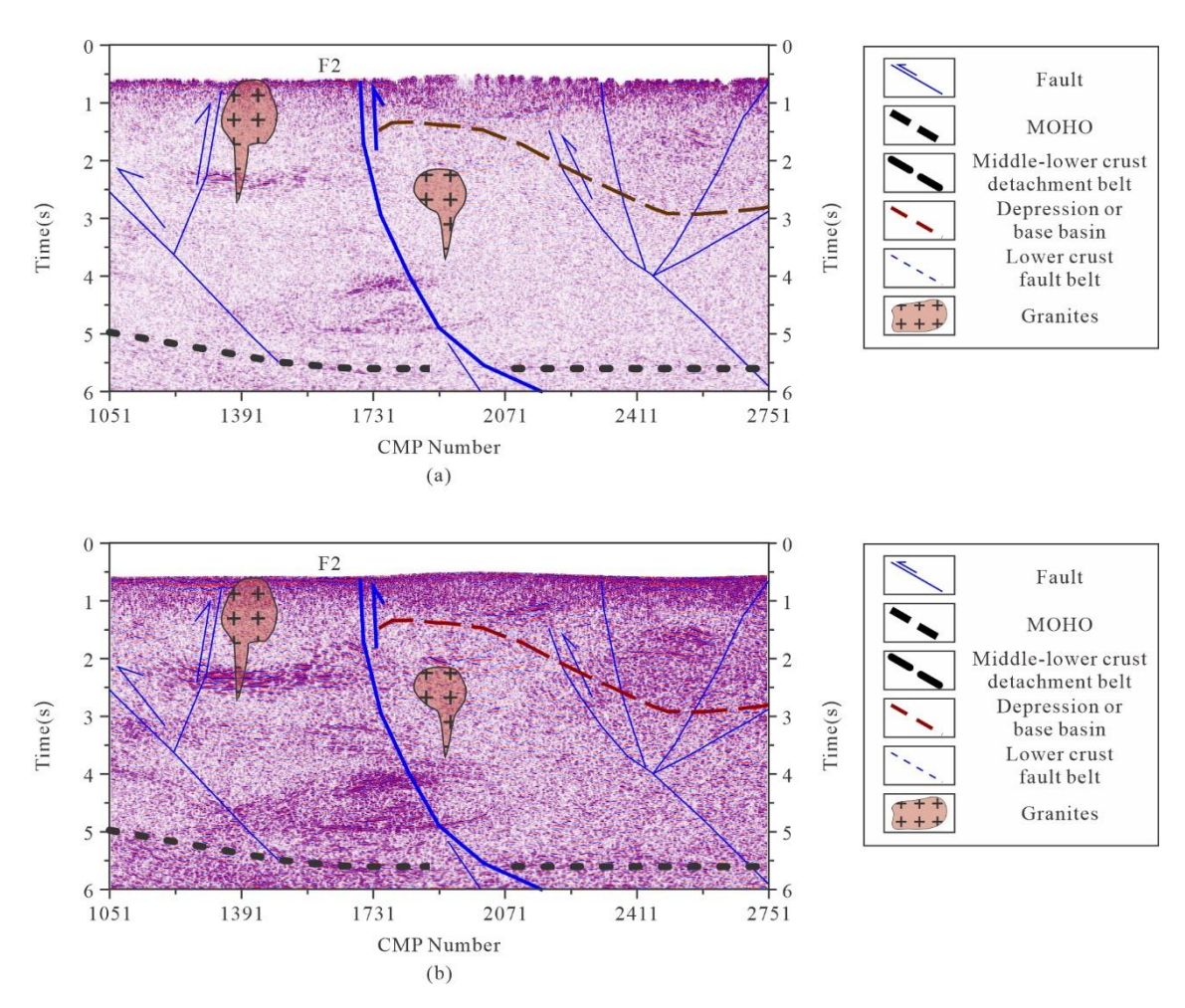


Figure 14 The shallow seismic profiles after pre-stack time migration. (a) before regularization, (b) after regularization and infilling shot gathers in the shot domain.





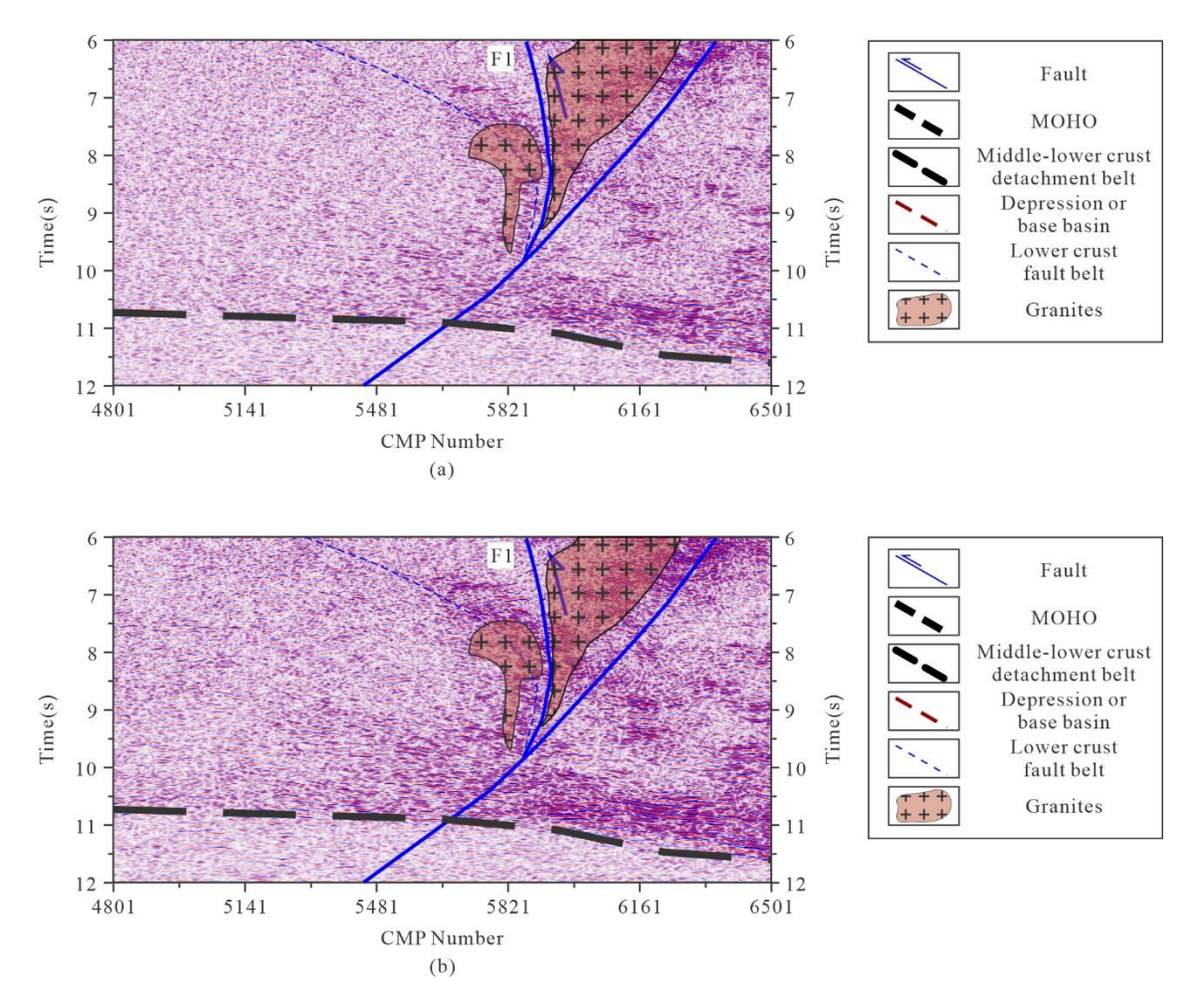


Figure 15 The deep seismic profiles after pre-stack time migration. (a) before regularization, (b) after regularization and infilling shot gathers in the shot domain.

6 Conclusions

305

310

This study evaluated four data regularization methods based on anti-aliasing MPFI to address seismic image degradation caused by irregular sampling in deep seismic reflection acquisition: 1) Infilling gaps in the offset domain; 2) Full offset-domain regularization; 3) Regularizing shot positions to 200 m intervals; and 4) Regularizing shot positions and infilling shot gathers to 100 m intervals. These methods were applied to deep seismic profiles from the middle segment of the JOB (Wuning–Ji'an section). All four approaches improved seismic image quality, with Method 4 delivering the most significant enhancement. It produced more regular shot and receiver spacing, a more uniform offset distribution, and doubled the fold, leading to better S/N and clearer imaging of both shallow and deep structures. Compared to contractor-processed stack profiles, Method 4 also yielded superior results in pre-stack time migration, with reduced migration noise and sharper structural images. These outcomes highlight the importance of regularization in deep seismic reflection workflows. Overall, regularization of Method

https://doi.org/10.5194/egusphere-2025-4554 Preprint. Discussion started: 15 October 2025

© Author(s) 2025. CC BY 4.0 License.



EGUsphere Preprint repository

4 proves to be an effective preprocessing step that enhances image quality, facilitates reliable data migration, and supports accurate interpretation of deep subsurface structures, contributing to more precise prediction of metal-rich zones.

Data availability

To request the data associated with this research, contact the corresponding author of the article after the publication of this work.

320 Author contributions

Hui Zhang: problem design and formulation, data analysis, results and discussion and manuscript writing. Jiayong Yan: data analysis, suggested and verified the results and discussion. Zhendong Liu: data analysis, suggested and verified the results and discussion. Jianguang Han: data analysis, suggested and verified the results and discussion. Hao Wang: figures design and manuscript corrections. Jiahao Liu: commented on the manuscript.

325 Competing interests

The authors declare no competing interests.

Acknowledgements.

We gratefully acknowledge the valuable feedback provided by anonymous reviewers and the strong support from the editorial team.

330 Funding

This study is supported by Deep Earth Probe and Mineral Resources Exploration - National Science and Technology Major Project (2024ZD1001202,2024ZD1002201), National Natural Science Foundation of China (42004179, U2344220) and the Deep Geological Survey Project of the China Geological Survey (DD20230008, DD20221656, DD20240079).

References

Ahmadi, O., Juhlin, C., Ask, M., and Lund, B.: Revealing the deeper structure of the end-glacial Pärvie fault system in northern Sweden by seismic reflection profiling, Solid Earth, 6, 621-632, 10.5194/se-6-621-2015, 2015.





- Bezerra, Y. S. F., Garabito, G., Sacchi, M., and Caldeira, J.: Data reconstruction combining MWNI and CRS-based interpolation methods, Journal of Applied Geophysics, 209, 104912, https://doi.org/10.1016/j.jappgeo.2022.104912, 2023.
- Cary, P. W. and Lorentz, G. A.: Four-component surface-consistent deconvolution, GEOPHYSICS, 58, 383-392, 10.1190/1.1443421, 1993.
 - Chen, C. X., Yan, J. Y., Liu, W. Q., Luo, F., Zhang, C., Xu, Y., Cheng, Z. Z., and Wang, Y.: Differences in Crustal Structure and Composition in Wuling-Middle Part of Jiangnan Orogenic Belt: Based on Geochemical and Geophysical Anomalies, Acta Geoscientica Sinica, 43, 785-802, 10.3975/cagsb.2022.063001, 2022.
- Ding, Y. S. and Malehmir, A.: Reverse time migration (RTM) imaging of iron oxide deposits in the Ludvika mining area, Sweden, Solid Earth, 12, 1707-1718, 10.5194/se-12-1707-2021, 2021.
 - Gan, C. S., Wang, Y. J., Barry, T. L., Zhang, Y. Z., and Qian, X.: Late Jurassic high-Mg andesites in the Youjiang Basin and their significance for the southward continuation of the Jiangnan Orogen, South China, Gondwana Research, 77, 260-273, https://doi.org/10.1016/j.gr.2019.06.018, 2020.
- Gao, R., Wang, H. Y., Zeng, L. S., Zhang, J. S., Guo, T. L., Li, Q. S., Li, W. H., Li, P. W., and Guan, Y.: The crust structures and the connection of the Songpan block and West Qinling orogen revealed by the Hezuo-Tangke deep seismic reflection profiling, Tectonophysics, 634, 227-236, https://doi.org/10.1016/j.tecto.2014.08.014, 2014.
 - Geng, Y. S.: Neoproterozoic Era of South China Craton, in: Precambrian Geology of China, edited by: Zhai, M., Springer Berlin Heidelberg, Berlin, Heidelberg, 263-301, 10.1007/978-3-662-47885-1_7, 2015.
- Gonçalves, B. F. and Garabito, G.: Flexible layer-based 2D refraction tomography method for statics corrections, Journal of Applied Geophysics, 185, 104254, https://doi.org/10.1016/j.jappgeo.2021.104254, 2021.
 - Hou, Q., Zhou, W. J., Yu, Z. Q., Hu, T. Y., Zhao, G. C., Yang, X. Y., Zhao, T. P., Tang, C., Fu, J. M., Liu, L., and Lu, Y. Y.: Geochronology, petrogenesis and tectonic significance of two episodes of Neoproterozoic diabasic magmatism in South China: from orogenesis to intracontinental rifting, International Geology Review, 64, 3074-3098, 10.1080/00206814.2021.2012718, 2022.
- Hu, J., Yu, X. Q., Xiao, W. J., and Li, W.: Transpression in the Eastern Jiangnan Orogen and its implications for ductile deformation process and regional Tectonics of the South China block, Journal of Structural Geology, 186, 105199, https://doi.org/10.1016/j.jsg.2024.105199, 2024.
 - Jahn, B. M., Zhou, X. H., and Li, J. L.: Formation and tectonic evolution of Southeastern China and Taiwan: Isotopic and geochemical constraints, Tectonophysics, 183, 145-160, https://doi.org/10.1016/0040-1951(90)90413-3, 1990.
- Kazemi, N., Bongajum, E., and Sacchi, M. D.: Surface-Consistent Sparse Multichannel Blind Deconvolution of Seismic Signals, IEEE Transactions on Geoscience and Remote Sensing, 54, 3200-3207, 10.1109/TGRS.2015.2513417, 2016.
 Krishna, V. G. and Rao, V. V.: Processing and modelling of short-offset seismic refraction-coincident deep seismic reflection data sets in sedimentary basins: an approach for exploring the underlying deep crustal structures, Geophysical Journal International, 163, 1112-1122, 10.1111/j.1365-246X.2005.02792.x, 2005.



395



- Lan, N. Y., Zhang, F. C., and Li, C. H.: Robust high-dimensional seismic data interpolation based on elastic half norm regularization and tensor dictionary learning, Geophysics, 86, V431-V444, 10.1190/geo2020-0784.1, 2021.
 - Li, L. M., Lin, S. F., Xing, G. F., Davis, D. W., Jiang, Y., Davis, W., and Zhang, Y. J.: Ca. 830Ma back-arc type volcanic rocks in the eastern part of the Jiangnan orogen: Implications for the Neoproterozoic tectonic evolution of South China Block, Precambrian Research, 275, 209-224, https://doi.org/10.1016/j.precamres.2016.01.016, 2016.
- Li, X. H., Li, Y. X., Wang, J. Y., Zhang, C. K., Wang, Y., and Liu, L.: Temporospatial variation in the late Mesozoic volcanism in southeast China, Solid Earth, 10, 2089-2101, 10.5194/se-10-2089-2019, 2019.
 - Liu, G. F., Meng, X. H., and Sea, J. G.: Case study: Improving the quality of the seismic reflection image for a Fujian mineral exploration data set with offset-domain common-image gathers, Geophysics, 86, B277-B289, 10.1190/geo2019-0770.1, 2021.
 - Liu, J. H., Yong, F., Liu, Z. D., Zhang, H., and Yan, J. Y.: Crustal Structure Characteristics of the Middle Part of Jiangnan
- Orogenic Belt: Insights from Random Medium Correlation Length Analysis of Wuning–Ji'an Deep Seismic Reflection Profile, Acta Geoscientica Sinica 43, 803-816, 10.3975/cagsb.2022.062601, 2022.
 - Liu, J. N., Huang, X. L., Xia, X. Y., and Li, X. P.: U-Pb and Hf Isotopic Analyses for Detrital Zircon of the Danzhou Group in the Western Jiangnan Orogenic Belt and Tectonic Implications, Minerals, 15, 10.3390/min15010070, 2025.
- Lu, Z. W., Gao, R., Guo, X. Y., Li, W. H., Xu, X., Shi, Z. X., Cheng, Y. Z., Wu, G. W., and Cai, Y. G.: The funnel-shaped crustal architecture in central Tibet and its insights into the progression of lithospheric removal, Geology, 53, 587-591, 10.1130/g52955.1, 2025.
 - Lu, Z. W., Guo, X. Y., Gao, R., Murphy, M. A., Huang, X. F., Xu, X., Li, S. Z., Li, W. H., Zhao, J. M., Li, C. S., and Xiang, B.: Active construction of southernmost Tibet revealed by deep seismic imaging, Nature Communications, 13, 3143, 10.1038/s41467-022-30887-3, 2022.
- 390 Luo, F., Lü, Q. T., Zhang, K., Yan, J. Y., Farquharson, C. G., Zhang, C., and Fu, G. M.: Crustal Electrical Structure and Deep Metallogenic Potential in Northern Wuyi Area (South China), based on Magnetotelluric Data, Acta Geologica Sinica-English Edition, 96, 791-805, 10.1111/1755-6724.14864, 2022.
 - Lü, Q. T., Yan, J. Y., Shi, D. N., Dong, S. W., Tang, J. T., Wu, M. A., and Chang, Y. F.: Reflection seismic imaging of the Lujiang–Zongyang volcanic basin, Yangtze Metallogenic Belt: An insight into the crustal structure and geodynamics of an ore district, Tectonophysics, 606, 60-77, 10.1016/j.tecto.2013.04.006, 2013.
 - Mao, X., Ye, G. F., Zhang, Y. X., Jin, S., and Wei, W. B.: Electric structure of the southern section of the Jiangnan orogenic belt and its tectonic implications, Chinese Journal of Geophysics-Chinese Edition, 64, 4043-4059, 10.6038/cjg2021O0424, 2021.
- Markovic, M., Maries, G., Malehmir, A., von Ketelhodt, J., Bäckström, E., Schön, M., and Marsden, P.: Deep reflection seismic imaging of iron-oxide deposits in the Ludvika mining area of central Sweden, Geophysical Prospecting, 68, 7-23, 10.1111/1365-2478.12855, 2019.
 - Naghizadeh, M., Snyder, D., Cheraghi, S., Foster, S., Cilensek, S., Floreani, E., and Mackie, J.: Acquisition and Processing of Wider Bandwidth Seismic Data in Crystalline Crust: Progress with the Metal Earth Project, 10.3390/min9030145, 2019.





- Panea, I., Prisacari, S., Mocanu, V., Micu, M., and Paraschivoiu, M.: The use of seismic modeling for the geologic interpretation of deep seismic reflection data with low signal-to-noise ratios, Interpretation, 5, T23-T31, 10.1190/int-2016-0046.1, 2017.
 - Schonewille, M., Yan, Z., Bayly, M., and Bisley, R.: Matching pursuit Fourier interpolation using priors derived from a second data set, SEG Technical Program Expanded Abstracts 2013, 10.1190/segam2013-0956.1, 2013.
- Schonewille, M., Klaedtke, A., Vigner, A., Brittan, J., and Martin, T.: Seismic data regularization with the anti-alias anti-leakage Fourier transform, First Break, 27, 85-92, 10.3997/1365-2397.27.1304.32570, 2009.
 - Snyder, D. B., Bleeker, W., Reed, L. E., Ayer, J. A., Houle, M. G., and Bateman, R.: Tectonic and Metallogenic Implications of Regional Seismic Profiles in the Timmins Mining Camp, Economic Geology, 103, 1135-1150, 10.2113/gsecongeo.103.6.1135, 2008.
 - Sun, J. J., Shu, L. S., Santosh, M., and Wang, L. S.: Precambrian crustal evolution of the central Jiangnan Orogen (South
- China): Evidence from detrital zircon U-Pb ages and Hf isotopic compositions of Neoproterozoic metasedimentary rocks, Precambrian Research, 318, 1-24, https://doi.org/10.1016/j.precamres.2018.09.008, 2018.
 - Taner, M. T. and Koehler, F.: Surface consistent corrections, GEOPHYSICS, 46, 17-22, 10.1190/1.1441133, 1981.
 - Wang, J. and Li, Z. X.: History of Neoproterozoic rift basins in South China: implications for Rodinia break-up, Precambrian Research, 122, 141-158, https://doi.org/10.1016/S0301-9268(02)00209-7, 2003.
- Wang, X. L., Zhou, J. C., Chen, X., Zhang, F. F., and Sun, Z. M.: Formation and Evolution of the Jiangnan Orogen, Bulletin of Mineralogy, Petrology and Geochemistry, 36, 714-735, https://doi.org/10.3969/j.issn.1007-2802.2017.05.003, 2017.
 - Wu, T. T. and Xu, Y. S.: Inverting Incomplete Fourier Transforms by a Sparse Regularization Model and Applications in Seismic Wavefield Modeling, Journal of Scientific Computing, 92, 48, 10.1007/s10915-022-01906-8, 2022.
 - Xu, D. R., Deng, T., Chi, G. X., Wang, Z. L., Zou, F. H., Zhang, J. L., and Zou, S. H.: Gold mineralization in the Jiangnan
- Orogenic Belt of South China: Geological, geochemical and geochronological characteristics, ore deposit-type and geodynamic setting, Ore Geology Reviews, 88, 565-618, https://doi.org/10.1016/j.oregeorev.2017.02.004, 2017.
 - Yan, J. Y., Chen, H., Deng, J. Z., Yu, H., You, Y. X., Wen, Y. D., and Feng, M.: Lithospheric Conductivity Structure in the Middle Segment of the Jiangnan Orogenic Belt: Insights into Neoproterozoic Tectonic–Magmatic Processes, Lithosphere, 2024, lithosphere_2023_2325, 10.2113/2024/lithosphere_2023_325, 2024.
- 430 Yan, J. Y., Lü, Q. T., Zhang, Y. Q., Liu, W. Q., Wang, X., Chen, C. X., Xu, Y., and Liu, J. H.: The deep boundaries of Jiangnan orogenic belt and its constraints on metallogenic: From the understanding of integrated geophysics, Acta Petrologica Sinica, 38, 544-558, 10.18654/1000-0569/2022.02.16, 2022.
 - Yao, J. L., Shu, L. S., and Santosh, M.: Neoproterozoic arc-trench system and breakup of the South China Craton: Constraints from N-MORB type and arc-related mafic rocks, and anorogenic granite in the Jiangnan orogenic belt, Precambrian Research,
- 435 247, 187-207, 10.1016/j.precamres.2014.04.008, 2014.
 - Yao, J. L., Cawood, P. A., Shu, L. S., and Zhao, G. C.: Jiangnan Orogen, South China: A ~970–820 Ma Rodinia margin accretionary belt, Earth-Science Reviews, 196, 102872, https://doi.org/10.1016/j.earscirev.2019.05.016, 2019.



445



Zappalá, S., Malehmir, A., Kranis, H., Apostolopoulos, G., and Papadopoulou, M.: Insight into the tectonostratigraphy of the historic Kefalonia island (Greece): a reflection seismic survey, EGUsphere, 2024, 1-20, 10.5194/egusphere-2024-3783, 2024.

- Zhang, Z. H., Zhang, D., He, X. L., Hu, B. J., Zhu, X. Y., Du, Z. Z., Jlia, W. B., and Gong, X. D.: Biotite granodiorite age of Jiuling complex in Jiangxi Province and its limitation on the collision and splicing time of the Yangtze and Cathay plates, Geology in China, 48, 1562-1579, 10.12029/gc20210518, 2021.
 - Zhou, X. M. and Li, W. X.: Origin of Late Mesozoic igneous rocks in Southeastern China: implications for lithosphere subduction and underplating of mafic magmas, Tectonophysics, 326, 269-287, https://doi.org/10.1016/S0040-1951(00)00120-7, 2000.
 - Zhu, X. S., Gao, R., Li, Q. S., Guan, Y., Lu, Z. W., and Wang, H. Y.: Static corrections methods in the processing of deep reflection seismic data, Journal of Earth Science, 25, 299-308, 10.1007/s12583-014-0422-x, 2014.